Food and Chemical Toxicology 163 (2022) 112994

Contents lists available at ScienceDirect

Food and Chemical Toxicology

journal homepage: www.elsevier.com/locate/foodchemtox

A novel paraoxon imprinted electrochemical sensor based on MoS_2NPs@MWCNTs and its application to tap water samples

Ömer Saltuk Bölükbaşı [a], Bahar Bankoğlu Yola [b], Havva Boyacıoğlu [c], Mehmet Lütfi Yola [d,*]

[a] Iskenderun Technical University, Faculty of Engineering and Natural Sciences, Department of Metallurgical and Materials Engineering, Hatay, Turkey
[b] Iskenderun Technical University, Science and Technology Application and Research Laboratory, Hatay, Turkey
[c] Pamukkale University, Faculty of Engineering, Department of Chemical Engineering, Denizli, Turkey
[d] Hasan Kalyoncu University, Faculty of Health Sciences, Department of Nutrition and Dietetics, Gaziantep, Turkey

ARTICLE INFO

Handling Editor: Dr. Jose Luis Domingo

Keywords:
Paraoxon
Molecularly imprinting
Voltammetry
Nanocomposite
Food safety

ABSTRACT

Organophosphorus pesticides are widely utilized in agricultural fertility. However, their long-term accumulations result in serious damage to human health and ecological balance. Paraoxon (PAR) can block acetylcholinesterase in the human body, resulting in death. Thus, in this study, a molecularly imprinted electrochemical PAR sensor based on multiwalled carbon nanotubes (MWCNTs)/molybdenum disulfide nanoparticles (MoS_2NPs) nanocomposite (MoS_2NPs@MWCNTs) was proposed for selective tap water determination. A hydrothermal fabrication approach was firstly implemented to prepare MoS_2NPs@MWCNTs nanocomposite. Afterwards, the formation of PAR imprinted electrochemical electrode was performed on nanocomposite modified glassy carbon electrode (GCE) in presence of PAR as template and pyrrole (Py) as a monomer by cyclic voltammetry (CV) technique. Just after determining the physicochemical features of as-fabricated nanostructures by scanning electron microscopy (SEM), transmission electron microscopy (TEM), x-ray diffraction (XRD), Raman spectroscopy, and atomic force microscopy (AFM), the electrochemical behavior of the fabricated sensors was determined through CV, differential pulse voltammetry (DPV), and electrochemical impedance spectroscopy (EIS). The suggested imprinted electrode provided the acceptable limit of quantification (LOQ) and limit of detection (LOD) values of 1.0×10^{-11} M, and 2.0×10^{-12} M, respectively. As a consequence, the proposed PAR imprinted electrochemical sensor can be offered for the determining safe tap water and its utility.

1. Introduction

Pesticides, which are used for purposes such as protecting agricultural products from pathogens, increasing productivity, and improving quality, that can be ended up in the food chain, and thus the life cycle, from various sources such as streams, rivers, and soil, and threaten both human health and the environment due to their high stability and toxicity (Gopi et al., 2022). Moreover, overuses of pesticides has become an increasingly critical problem that threatens notably the environment, as well as human health (Paschoalin et al., 2022; Raymundo-Pereira et al., 2021). Organophosphate compounds, have a wide range of uses, including their use as insecticides, herbicides, and even as an agent in living organisms to transmit neurons (Dhull, 2020). Even more, it can serious complications since when it interacts with human beings it may cause respiratory disorders, atrial fibrillation, and even muscle dysfunction by inhibiting acetylcholinesterase enzymes (Costa et al., 2008; Mulchandani et al., 2001; Palleschi et al., 1992). There are a number of organophosphorus insecticides, one of which is paraoxon (PAR), exceedingly harmful to human health (Gallardo et al., 2006). With a half-life of around 5000 years, PAR is one of the most potent and toxic acetylcholinesterase insecticides and has various biological harmful side effects (Khoshsafar et al., 2022). Monitoring of even a trace amount of PAR in both environmental and human samples such as air, soil, water, urine, blood, etc. is seemed to be a solution to contain the pesticide contamination problem (Gopi et al., 2022). Although the performance of powerful analytical techniques such as chromatography and mass spectroscopy for PAR detection has been validated until now (Bravo et al., 2002; Ioerger and Smith, 1993), studies on the development of alternative methods have accelerated due to their costly, time-consuming and complex systems, the requirements of qualified personnel, and their inability to perform *in-situ* and real-time analysis (Gopi et al., 2022). Hence, high-performance electrochemical sensors

* Corresponding author.
E-mail address: mlutfi.yola@hku.edu.tr (M.L. Yola).

https://doi.org/10.1016/j.fct.2022.112994
Received 5 March 2022; Received in revised form 22 March 2022; Accepted 4 April 2022
Available online 7 April 2022

with high sensitivity, simplicity, cost-effective, fast response time, as well as being suitable for real-time analysis, are considered as one of the most effective methods for the detection of organic compounds including pesticides (Boke et al., 2020; Karimi-Maleh et al., 2022a, b; Karimi-Maleh et al., 2021a; Medetalibeyoglu et al., 2020; Mohanraj et al., 2020). It should be highlighted, however, that it is critical to enhance the sensitivity, selectivity, and repeatability of the bare electrode by modifying it with high-performance nanostructures (Karaman et al., 2022a, 2022b) In this respect, various forms of nanoarchitectures present a new avenue for altering electrodes to improve their electrochemical features, thanks to cutting-edge developments in nanotechnology.

Carbon nanotubes have been garnered a huge amount of concern in recent years for electrochemical determinations due to superior electronic conductivity, physicochemical properties, and specific surface area (Agui et al., 2008; Verma et al., 2021). Furthermore, carbon nanotubes can increase the ability of electron transfer between target molecules and electrode surface. Thus, they can be employed as the electrochemical materials for the fabrication of electrochemical sensor/biosensor (Lahiff et al., 2010). Recently, metal dichalcogenides with a layered structure such as SnS_2 and MoS_2 have been started a significant interest in electrochemical applications owing to excellent electronic structure and specific surface area (Huang et al., 2013b; Li et al., 2013a). Molybdenum disulfide (MoS_2) with its layered architecture is known to be a good functional material because of electron-electron interactions between molybdenum atoms providing the increase of electrochemical transportation efficiency. MoS_2 is composed of the sandwiched molybdenum atom between two sulfur atoms and possesses poor van der Waals interactions through layers (Li et al., 2013b; Yin et al., 2012). In addition, MoS_2 can be employed in a variety of applications such as catalysts, supercapacitor, and lithium battery (Ma et al., 2013; Rezaei et al., 2012). However, due to MoS_2's limited electronic conductivity in comparison with graphene oxide/graphene, many efforts have been spent on the improvement of sensor electrode material efficiency (Ma et al., 2013). Nonetheless, the doping or combination treatment between MoS_2 and some conducting materials can eliminate the limited electronic conductivity. For example, polypyrrole/MoS_2 composites were synthesized and utilized as an electrode material in supercapacitor application (Ma et al., 2013). Lastly, the voltammetric sensor based on graphene/MoS_2 was also presented to detect acetaminophen, dopamine, and ascorbic acid (Huang et al., 2013a).

In this work, a molecularly imprinting electrochemical paraoxon sensor based on MoS_2NPs@MWCNTs nanocomposite was proposed for the first time. First of all, the preparation of MoS_2NPs, and MoS_2NPs@MWCNTs nanostructures was performed by a hydrothermal technique. Subsequently, the molecular imprinting technique (MIT) was carried out on MoS_2NPs@MWCNTs nanocomposite. Since it can replicate natural recognition entities such as antibodies and biological receptors, MIT is a promising synthetic strategy for designing molecular recognition technologies. This technique based on molecular recognition is a kind of polymerization process that occurs around relevant molecules called target molecules and creates specific cavities with highly cross-linked polymeric matrices (Beytur et al., 2018; Karimi-Maleh et al., 2021b; Ozkan et al., 2019). The construction of molecularly imprinted polymer (MIP) generally consists of three steps: (i) an interaction between the functional monomers and the template molecule, (ii) Cross-linking polymerization process with monomer-target molecule, (iii) Desorption of the target molecule with a desorption agent. As a consequence of this work, it was revealed that the developed MIP-based electrochemical sensor could provide high selectivity, superior sensitivity with a LOD of 2.0×10^{-12} M, good health and environmental compatibility.

2. Experimental

2.1. Materials

Paraoxon (PAR), lindane (LIN), chlorpyrifos (CHL), methyl parathion (MEPA), malathion (MAL), uric acid (UA), MWCNTs (with 20–30 nm in diameter and 1.0–4.0 mm in length), cetyltrimethylammonium bromide (CTAB), sodium molybdate dihydrate ($Na_2MoO_4.2H_2O$), pyrrole, and L-cysteine were supplied from Sigma-Aldrich. In addition to be utilized as a dilution buffer solution, a 1.0×10^{-1} M phosphate-buffered saline (PBS) (pH = 7.0) was employed as a supporting electrolyte.

2.2. Apparatus

ZEISS EVO 50 SEM (Carl-Zeiss-Stiftung, Germany), and JEOL 2100 TEM (JEOL Ltd., Tokyo, Japan) were employed to examine the surface morphologies of nanostructures. The XRD survey of the nanomaterials were recorded through a Rigaku X-ray diffractometer (MiniFlex, Japan/USA) with Cu-Kα radiation (λ = 0.154 nm). Furthermore, the Gamry Reference 600 workstation (Gamry, USA) was assigned with performing CV, EIS, and DPV investigations for the electrochemical characterizations.

2.3. Fabrication procedure of MoS_2NPs and MoS_2NPs@MWCNTs nanostructures

A hydrothermal production approach was applied for the fabrication of MoS_2NPs and MoS_2NPs@MWCNTs nanocomposite (Yadav et al., 2021). Firstly, MWCNTs (20.0 mg) and CTAB (200.0 mg) was dispersed in ultra-pure water (100.0 mL) at 25 °C. CTAB as cationic surfactant provided homogeneous dispersion of nanotubes. Following that, $Na_2MoO_4.2H_2O$ (0.60 g) was poured into the nanotubes dispersion and ultra-sonicated over 30 min. After the adjustment of pH to 7.0 with 0.1 M NaOH solution, L-cysteine (1.00 g) was also added into the resultant dispersion. After vigorious stirring for 30 min, the mixture was transported to Teflon steel autoclave and the maintained at 200 °C for 20 h, providing ***MoS_2NPs@MWCNTs*** nanocomposite. The preparation of ***MoS_2NPs*** was performed by same fabrication procedure without introducing MWCNTs.

2.4. Fabrication of MoS_2NPs@MWCNTs nanocomposite modified GCE

Following the previously described cleaning procedure, the as-cleaned GCE was kept ready for its upcoming use (Yola et al., 2012). Briefly, in the cleaning procedure of GCE, Al_2O_3 slurries of various particle sizes were deposited onto polishing pads, and GCE was treated with them over a 10 min. Following the rinsing of GCE with acetonitrile at 25 °C to eliminate residual alumina on the GCE, the MoS_2NPs@MWCNTs dispersion (20.0 μL, 0.2 mg mL^{-1}) was gently dropped onto the as-cleaned GCE surface. Afterwards, an IR heat lamp was employed for 30 min to remove the solvent from GCE surface, resulting in MoS_2NPs@MWCNTs modified GCE (***MoS_2NPs@MWCNTs/GCE***) as electrochemical sensor platform. Finally, the same procedure was implemented to fabricate MWCNTs modified GCE (***MWCNTs/GCE)***.

2.5. Molecular imprinting of PAR on MoS_2NPs@MWCNTs/GCE and the studies of PAR removal from the electrode surface

The molecular imprinting of PAR on MoS_2NPs@MWCNTs/GCE (***MIP/MoS_2NPs@MWCNTs/GCE***) was carried out in the presence of 100.0 mM Py as a monomer in 25.0 mM PAR contained PBS solution (0.1 M, pH = 7.0). This was conducted by 30 subsequent CV cycle at 100 mV s^{-1} potential scan rate and in the potential range of +0.30 V to +1.20 V. PAR non-imprinted polymer on MoS_2NPs@MWCNTs/GCE (***NIP/MoS_2NPs@MWCNTs/GCE***) was also successfully prepared by the

same fabrication procedure except for introducing PAR into PBS solution. Moreover, for comparison, the same protocol was also performed to fabricate MIP/bare GCE and MIP/MWCNTs/GCE. Scheme 1 illustrated the fabrication procedure of MoS_2NPs@MWCNTs nanocomposite and PAR imprinted electrochemical electrode. There are specific electrostatic forces, and hydrogen bond interactions between the Py's polar groups and PAR molecules. Hence, these interactions were need to be eliminated. In this regard, all PAR imprinted electrodes were firstly placed into shaker containing 20.0 mL NaCl solution (1.0 mol L^{-1}) as a desorption agent, following by it was shaked at 250 rpm during elution time of 20 min. Subsequently, the prepared PAR imprinting electrodes were allow to dry at the ambient temperature. A three-electrode system including Ag/AgCl (sat KCl) as reference, platinum wire as counter electrode and MIP/MoS_2NPs@MWCNTs/GCE as working electrode was used in all electrochemical experiments. Argon gas (>99,9%) was passed through the solution 100.0 mM Py in 25.0 mM PAR contained PBS solution (0.1 M, pH = 7.0) during 15 min before the elimination of O_2.

2.6. Procedure for real sample preparation

The tap water samples were acquired from a local tap in Gaziantep/TURKEY. The samples were employed in experiments without any filtration to show the applicability of the proposed PAR imprinted electrode. In addition, pH adjustment of the samples was implemented by 0.1 M acetic acid.

3. Results and discussion

3.1. Principle of MoS_2NPs@MWCNTs nanostructure preparation

A hydrothermal technique was implemented to prepare the MoS_2NPs and MoS_2NPs@MWCNTs nanostructures. The hydrothermal technique is of several advantages including minimal chemical consumption and cost-efficiency (Pourabbas and Jamshidi, 2008). In addition, this technique can provide the controlled growth of nanoparticles and the controlled nucleation (Hu et al., 2007; Wang et al., 2004). Owing to the low crystallinity of MoS_2NPs, the complex structure between MoS_2NPs and MWCNTs occurred under hydrothermal conditions (Pourabbas and Jamshidi, 2008). MWCNTs providing the promotion of MoS_2NPs growth on its surface caused the formation of the layered structure of MoS_2NPs with the high crystallinity degree. Due to the incorporation of MoS_2NPs into MWCNTs, the improved chemical, physical and mechanical properties were observed, providing that MoS_2NPs@MWCNTs nanocomposite acted as the efficient functional material for sensor applications. Furthermore, L-cysteine acted as the sulfur source and a reducing agent during nanocomposite preparation. Thus, H_2S was released, indicating the reduction of MoO_4^{2-} into MoS_2. The reaction mechanism can be expressed as follows (Huang et al., 2014; Pourabbas and Jamshidi, 2008):

$$HSCH_2CHNH_2COOH + H_2O \rightarrow CH_3COCOOH + NH_3 + H_2S \quad (1)$$

$$4MoO_4^{2-} + 9H_2S + 6CH_3COCOOH \rightarrow MoS_2 + SO_4^{2-} + 6CH_3COCOO^- + 12H_2O \quad (2)$$

3.2. Characterizations of MoS_2NPs and MoS_2NPs@MWCNTs nanostructures

XRD studies were firstly carried out to explore the crystalline

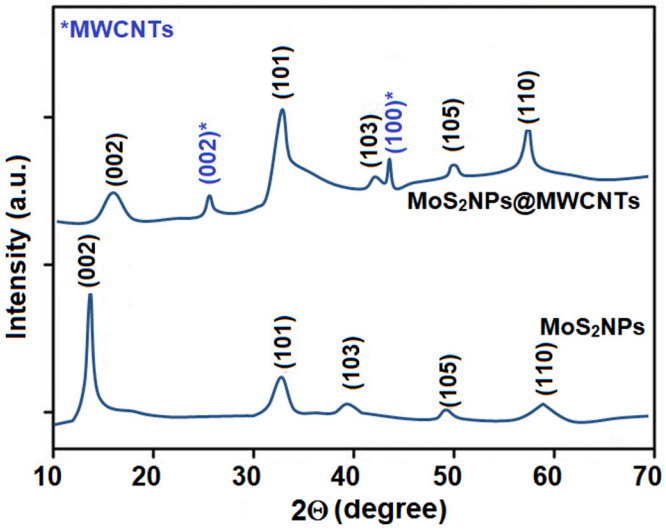

Fig. 1. XRD spectra of MoS_2NPs and MoS_2NPs@MWCNTs nanocomposite.

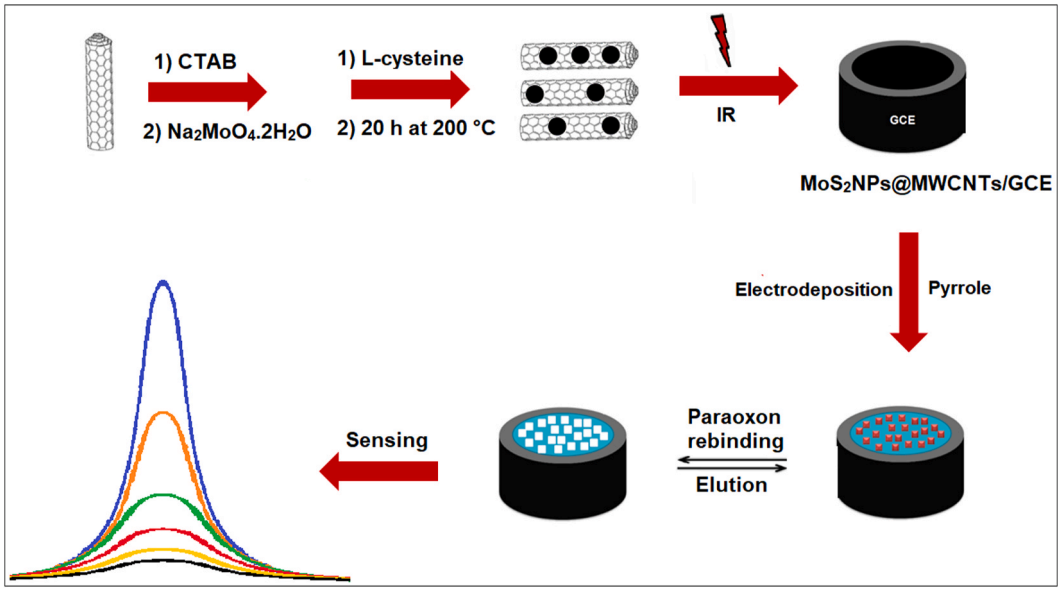

Scheme 1. Preparation protocol of MoS_2NPs@MWCNTs nanocomposite and PAR imprinted electrochemical electrode.

structures of MoS_2NPs and MoS_2NPs@MWCNTs nanostructures (Fig. 1). The whole specific XRD peaks relating to MoS_2NPs were observed in the hexagonal phase due to XRD peaks attributing to (002), (101), (103), (105) and (110) crystal planes which were corresponded to $2\theta = 13.94°$, 33.44°, 40.18°, 50.07°, and 59.04°, respectively (Liu et al., 2016). In addition, the XRD pattern of MWCNTs was also represented in Fig. S1. According to Fig. S1, the XRD peaks detected at $2\theta = 26.09°$, and 43.41° corresponded to (002), and (100) planes, respectively, and were attributed to graphite's hexagonal structure, indicating the superior electrochemical conductivity of MWCNTs. XRD peaks belonging to MoS_2NPs were detected on XRD pattern of MoS_2NPs@MWCNTs nanocomposite. On the other hand, the intensities of XRD peaks belonging to MWCNTs were weak, suggesting the full incorporation of MoS_2NPs into MWCNTs surface (Huang et al., 2014). Furthermore, the XRD peak belonging to (002) plane of MoS_2NPs@MWCNTs nanocomposite was shifted to a higher angle in comparison with MoS_2NPs. Hence, it was concluded that the preparation of MoS_2NPs on MWCNTs surface was confirmed via the lattice expansion in the c-axis direction.

Raman spectra (Fig. S2) was collected for the evaluation of the electronic and structural properties of MoS_2NPs@MWCNTs nanocomposite. The absorption peaks at 410 cm^{-1} (A_{1g}), and 377 cm^{-1} (E^1_{2g}) were observed in harmony with out-of-plane and in-plane modes of MoS_2NPs. These absorption peaks revealed that MoS_2NPs structure was parallel to 2H–MoS_2 (Lee et al., 2010). In addition, for MWCNTs, the detected D band at 1346 cm^{-1}, and G band at 1586 cm^{-1} were corresponded to sp3-hybridized carbon, and E^1_{2g} mode, respectively, (Huang et al., 2014). Hence, the successful synthesis of MoS_2NPs on MWCNTs was confirmed by also the Raman spectra of the nanostructures.

The measurement of zeta potential was also conducted to explore the overall charge on MoS_2NPs@MWCNTs nanostructure (Fig. S3). According to Fig. S3, MoS_2NPs@MWCNTs was of about 28 mV positive charge, attributing to the presence of CTAB on the surface. The bounded CTAB group resulted in this positive charge, and it provided a smooth film of MoS_2NPs@MWCNTs nanostructure on glassy carbon electrode.

TEM images (Fig. 2) were obtained to further examine the surface morphology of MoS_2NPs, and MoS_2NPs@MWCNTs nanostructures. According to Fig. 2A, the twisted thin layers belonging to MoS_2NPs were observed. In addition, TEM micrograph of MoS_2NPs@MWCNTs nanocomposite (Fig. 2B) demonstrated that the uniform grown of MoS_2NPs on the surface of MWCNTs was successfully accomplished. Hence, the insertion of MWCNTs between MoS_2NPs layers was confirmed. According to Fig. 2C, the distribution and interconnection of MoS_2NPs layers on MWCNTs surface resulted in a three-dimensional nanostructure. During hydrothermal process, MWCNTs had significant function as substrate to carry out MoS_2NPs' growth and nucleation on carbon nanotube surface. HRTEM image (Fig. 2D) of MoS_2NPs@MWCNTs nanocomposite showed the interface between MoS_2NPs and MWCNTs. The space interlayer distances of MoS_2NPs and MWCNTs were calculated as 0.50 nm and 0.38 nm, respectively (Fig. 2D).

SEM images were provided for the investigation of surface properties. According to Fig. 3A, MWCNTs was smooth and homogeneous in harmony with specific nanotube morphology. Fig. 3B demonstrated flexible wrinkled sheets belonging to MoS_2NPs. Three-dimensional structure of MoS_2NPs@MWCNTs nanocomposite was observed on Fig. 3C, confirming the insertion of MoS_2NPs into MWCNTs. Hence, this structural difference provided a high surface-to-volume ratio which improved the electrochemical surface area. Furthermore, MoS_2NPs' incorporation into nanocomposite structure gained an interlinked conducting framework providing a feasible way for the electron transfer.

AFM measurements (Fig. S4) were carried out for the examination of the thickness and surface morphology. Fig. S4A showed the AFM image of bare GCE with a roughness value of 2.60 nm whereas Fig. S4B demonstrated the AFM image of MoS_2NPs@MWCNTs nanocomposite modified GCE. Fig. S4B confirmed the homogenous and uniform topography of nanostructure and its roughness value was calculated as 13.44 nm. Thus, the observed morphological change confirmed the successful modification of GCE by MoS_2NPs@MWCNTs nanostructure.

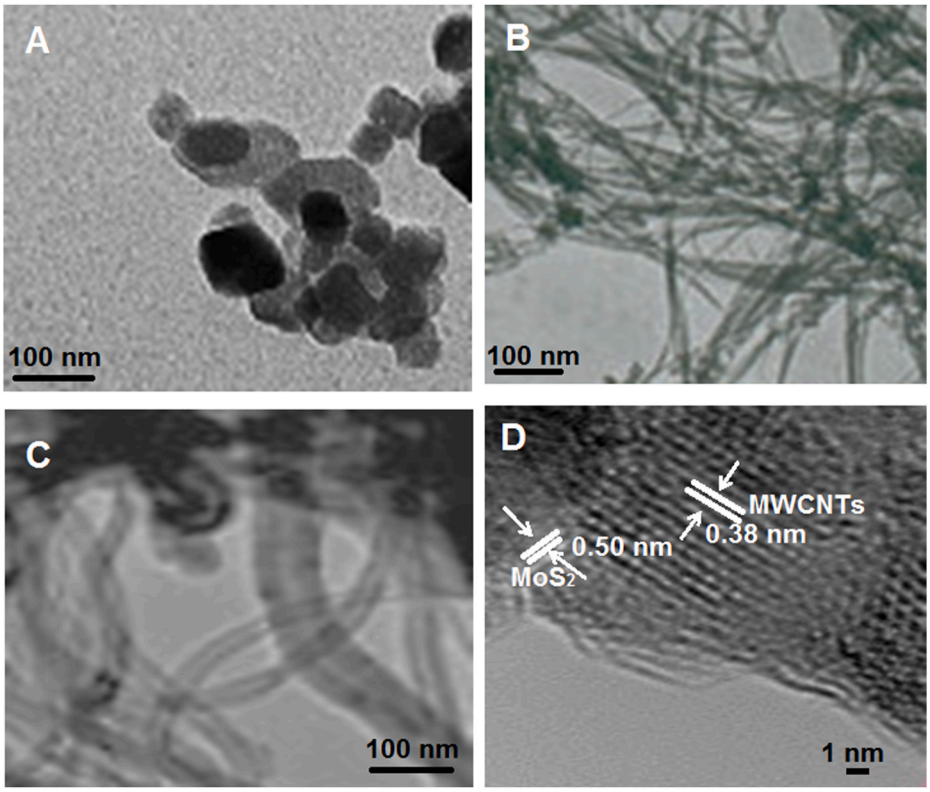

Fig. 2. TEM image of (A) MoS_2NPs, (B) and (C) MoS_2NPs@MWCNTs nanocomposite, (D) HRTEM image of MoS_2NPs@MWCNTs nanocomposite.

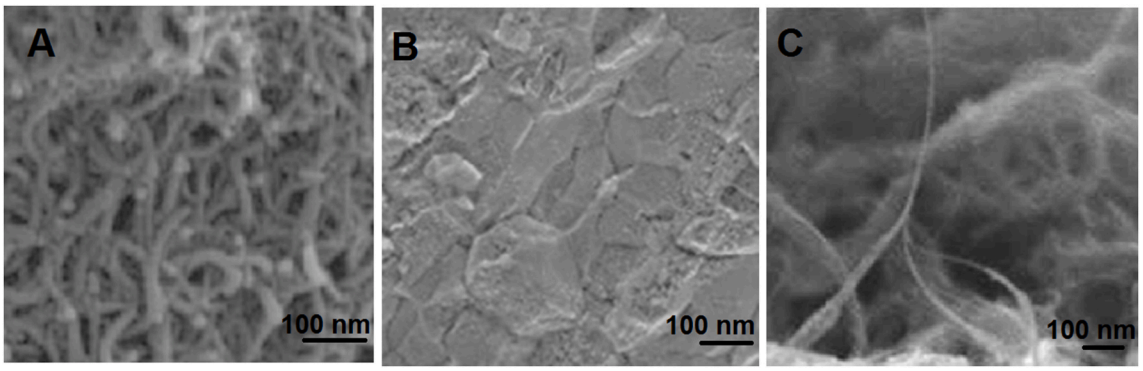

Fig. 3. SEM image of (A) MWCNTs, (B) MoS_2NPs and (C) MoS_2NPs@MWCNTs nanocomposite.

3.3. Assessment of electrochemical behaviors of MWCNTs and MoS_2NPs@MWCNTs nanostructure modified electrodes

The electrochemical characteristics of the as-constructed sensor platforms were evaluated by means of CV and EIS techniques in the presence of 1.0 mM $[Fe(CN)_6]^{3-/4-}$. Initially, an anodic peak at +0.300 V and a cathodic peak at +0.150 V were detected using bare GCE (curve a of Fig. 4A). On the other hand, for MWCNTs/GCE (curve b of Fig. 4A), an obvious enhancement in the electrochemical response was detected owing to its electronic, chemical characteristics, besides its large surface area (Agui et al., 2008; Xu and Wang, 2005). When MoS_2NPs@MWCNTs nanocomposite modified electrodes (curve c of Fig. 4A) were exposed to 1.0 mM $[Fe(CN)_6]^{3-/4-}$, the electrochemical performances were augmented over MWCNTs/GCE due to the synergistic impact of MoS_2NPs and carbon-based materials.(Huang et al., 2013a).

In order to verify CV results, EIS measurements were subsequently implemented (Fig. 4B). The charge transfer resistance (R_{ct}) values of bare GCE (curve a), MWCNTs/GCE (curve b), and MoS_2NPs@MWCNTs/GCE (curve c) were determined as 90 Ω, 75 Ω, and 60 Ω, respectively. As a consequence, the most efficient charge transfer occurred on MoS_2NPs@MWCNTs/GCE due to its relatively lower R_{ct} value. Ultimately, the data revealed that the CV and EIS results were in good agreement.

3.4. Polymerization of PAR imprinted polymer on MoS_2NPs@MWCNTs/GCE

Fig. S5A demonstrated the polymerization voltammograms in the existence of 100.0 mM Py containing 25.0 mM PAR on MoS_2NPs@MWCNTs/GCE. The electrooxidation current signals were observed at 1.0 V during the 1st scan cycle. Following then, the current signals rapidly decreased with succeeding scans, virtually disappearing in the 30th cycle. It was concluded that these decreasing peak current signals indicated polymer formation on MoS_2NPs@MWCNTs/GCE.

Differential pulse voltammograms (DPVs) were obtained by using MIP/MoS_2NPs@MWCNTs/GCE and NIP/MoS_2NPs@MWCNTs/GCE to verify the imprinting selectivity (Fig. S5B). As expected, there were no obvious electrochemical signals observed without PAR molecules (curve a of Fig. S5B). When the electrochemical signals between NIP and MIP surfaces were compared, the current signals on MIP/MoS_2NPs@MWCNTs/GCE (curve c of Fig. S5B) were found to be higher than those of NIP/MoS_2NPs@MWCNTs/GCE (curve b of Fig. S5B) in presence of 0.5 nM PAR in 0.1 M PBS (pH 7.0). As a result, the considerable selectivity property was provided in this work by applying molecular imprinting technology.

Finally, identical PAR imprinted electrochemical electrodes were constructed and tested in 1.0×10^{-1} mol.L^{-1} PBS with 0.5 nM PAR. In agreement with Fig. 4A and B, the strongest current signals were detected on MIP/MoS_2NPs@MWCNTs/GCE, as shown in Fig. S5C. In addition, according to Fig. S6 including PAR electroreduction, an electrochemical reaction with an equal number of electrons and protons occurred (Gopi et al., 2022).

The SEM micrographs of MIP and NIP surfaces were also provided for morphological evaluation (Fig. S7). According to Fig. S7A, the porous polymeric structures were observed, indicating a successful polymerization process. On the contrary, smooth polymeric structures were shown in Fig. S7B, confirming NIP formation on the electrode surface.

3.5. Optimization investigations

In optimization experiments, the effects of solution pH, molar ratios of PAR to pyrrole monomer, desorption duration, and scan cycle were

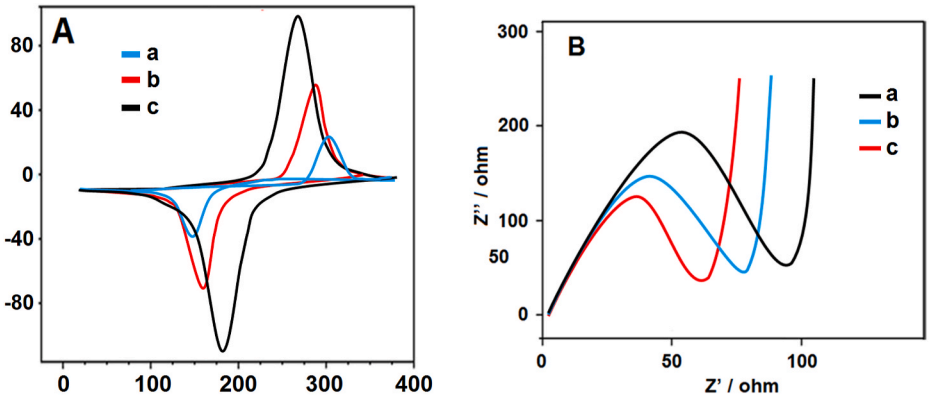

Fig. 4. (A) CV curves and (B) EIS responses at (a) bare GCE, (b) MWCNTs/GCE, (c) MoS_2NPs@MWCNTs/GCE, (Redox probe: 1.0 mM $[Fe(CN)_6]^{3-/4-}$ containing 0.1 M KCl, potential scan rate: 100 mV s^{-1}).

thoroughly explored and were reported in Supplementary Materials (Fig. S8).

3.6. Linearity range

The acquired calibration equation of y (μA) = 15.911x (C_{PAR}, nM) + 0.0514, (R^2 = 0.9997) by increasing PAR concentrations and differential pulse signals were depicted in Fig. 5. LOQ, and LOD values were computed as 1.0×10^{-11} M, and 2.0×10^{-12} M, respectively, by means of equations (3) and (4):

$$LOQ = 10.0\ S / m \quad (3)$$

$$LOD = 3.3\ S / m \quad (4)$$

where S represents the standard deviation of the intercept, whereas m stands for the slope of the regression line. Table 1 demonstrated how the developed electrochemical PAR sensor outperformed previous approaches in terms of sensitivity and linearity. First of all, a hydrothermal technique was applied for the preparations of MoS_2NPs and MoS_2NPs@MWCNTs nanocomposite. This synthesis method has several advantages including minimal chemical consumption and cost-efficiency. In addition, a sensitive PAR imprinted electrode was prepared in the present work in the terms of LOD values. The other advantage issue was satisfactory selectivity in real sample analysis via the molecularly imprinting technique. Hence, it can be speculated that in this work, the molecularly imprinted electrode system with high selectivity, sensitivity, and stability was presented for high-efficiency PAR assay.

3.7. Recovery analysis

Tap water samples were prepared for the recovery studies. Table S1 tabulated the recovery values of PAR in the existence of 1.0×10^{-1} M PBS solution (pH 7.0), which were obtained by Equation (5).

Recovery = Found PAR, nM/Real PAR, nM (5).

According to Table S1 of recovery experiments, the values close to 100.00% confirmed the high accuracy of the as-fabricated molecularly imprinting electrode, thereby revealing the effective determination of PAR in tap water samples without any interference effect.

Standard addition method was also tried to confirm the high selectivity for tap water samples and y (μA) = 15.937x (C_{PAR}, nM) + 1.173 R^2 = 0.9991 was formed as calibration equation. Thereby, the close slope values between direct calibration (inset of Fig. 5) and standard addition methods suggested the selective PAR assay.

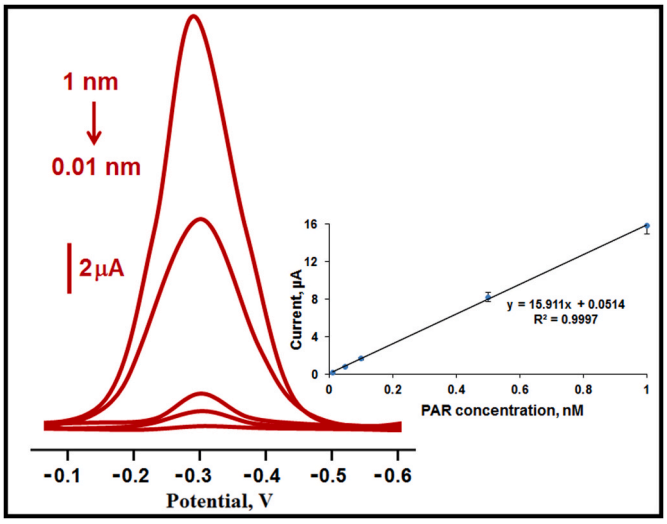

Fig. 5. DPVs with different PAR concentrations at MIP/MoS_2NPs@MWCNTs/GCE in PBS with pH = 7.0 (in a concentration range of 0.01–1.0 nM). Inset: PAR's calibration curve.

Table 1
The performance characteristics of the as-fabricated electrochemical PAR sensor in comparison to those of different recently described approaches.

Material or Method	Linear Range (M)	LOD (M)	Ref.
Stearic acid/nanosilver/GCE	1.0×10^{-10} – 5.0×10^{-9}	1.0×10^{-10}	Kumaravel et al. (2020)
PEDOT/PSS	0.0–8.0 × 10^{-7}	4.95 × 10^{-6}	Hryniewicz et al. (2018)
Bismuth film/GCE	5.0×10^{-9} – 4.0×10^{-8}	2.0 × 10^{-9}	Stoytcheva et al. (2017)
Graphene oxide encapsulated 3D porous chalcopyrite Modified SPCE	7.0×10^{-8} – 8.0×10^{-4}	4.5 × 10^{-9}	Rajaji et al. (2019)
OMCs/GCE	1.0×10^{-8} – 1.0×10^{-6}	1.9 × 10^{-9}	Zhang et al. (2014)
$BiVO_4$/SPCE	1.0×10^{-6} – 1.0×10^{-5}	3.0 × 10^{-8}	Gopi et al. (2022)
CuNCs@BSA-SWCNT	5.0×10^{-8} – 3.5×10^{-5}	1.3 × 10^{-8}	Bagheri et al. (2017)
CBNPs-DMF-Glut-Nf-BSA-BChE	2.0×10^{-8} – 1.2×10^{-7}	2.0 × 10^{-8}	Arduini et al. (2015)
MIP/MoS_2NPs@MWCNTs/GCE	***1.0×10^{-11} – 1.0×10^{-9}***	***2.0 × 10^{-12}***	***This study***

3.8. Assessment of the selectivity, stability, reproducibility and reusability features of the fabricated PAR imprinted electrode

For the selectivity assessment, six unique solutions including (i) 1.0 nM PAR, (ii) 100.0 nM LIN, (iii) 100.0 nM CHL, (iv) 100.0 nM MEPA, (v) 100.0 nM MAL, and (vi) 100.0 nM UA were prepared, and the fabricated PAR imprinted electrode was applied to them. According to Fig. 6A and Fig. 6B, the obtained current signals (μA) were observed as 16.0 μA, 0.80 μA, 0.60 μA, 0.40 μA, 0.30 μA, and 0.20 μA, for PAR, LIN, CHL, MEPA, MAL, and UA respectively, by using MIP/MoS_2NPs@MWCNTs/GCE. On the other hand, by using NIP/MoS_2NPs@MWCNTs/GCE, the current signals (μA) were determined as 1.0 μA, 0.40 μA, 0.30 μA, 0.20 μA, 0.10 μA, and 0.05 μA, for PAR, LIN, CHL, MEPA, MAL, and UA, respectively. Table S2 also summarized both the selectivity coefficient (k) and relative selectivity coefficient (k′) values. According to Table S2, the proposed PAR imprinted electrode was 20.00, 26.67, 40.00, 53.33 and 80.00 times more selective for PAR against LIN, CHL, MEPA, MAL and UA owing to selective cavities of PAR molecule in polymeric structure. As a consequence, we can infer that the molecular imprinting approach resulted in great selectivity in sensor applications with no interference impact.

The gathering of 7-week period DPV data demonstrated the stability of the suggested PAR imprinted electrode. (Fig. S9). The obtained current signal at the end of the 7th week was calculated as almost 99.02%, indicating the superior stability of the proposed PAR imprinted electrode.

For the repeatability tests, 20 separate PAR imprinted electrodes were constructed using the procedure outlined in sections 2.4 and 2.5. The relative standard deviation of the observed current signals was 0.18, confirming the high level of reliability.

Lastly, the reusability test for the proposed PAR sensor was presented. During the proposed one PAR sensor' 40 times usages, relative standard deviation (RSD) value of the obtained current (I) signals was calculated as 0.97%, confirming a high degree of reusability.

4. Conclusions

In the present work, a selective and precise molecularly imprinted electrochemical sensor based on MoS_2NPs@MWCNTs nanocomposite was presented for paraoxon assay. The proposed paraoxon imprinted

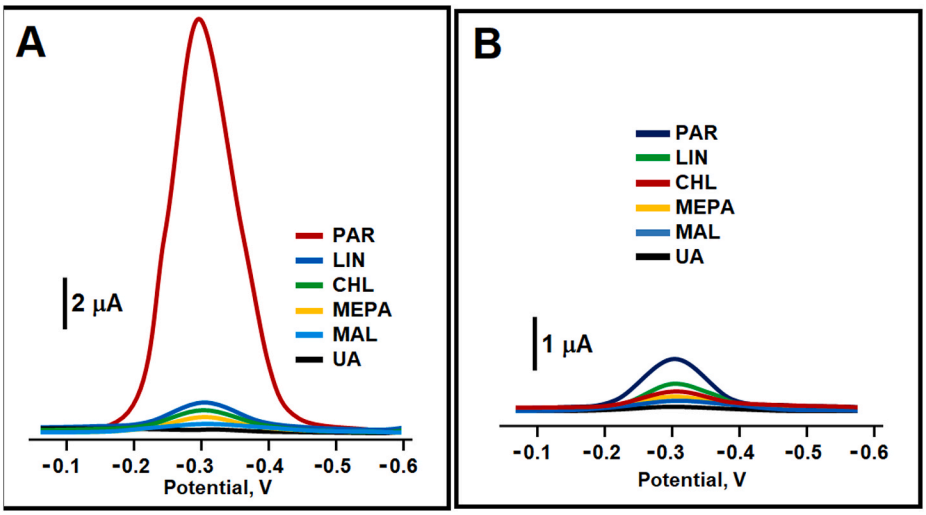

Fig. 6. DPVs of (A) MIP/MoS_2NPs@MWCNTs/GCE and (B) NIP/MoS_2NPs@MWCNTs/GCE in 1.0 nM PAR, 100.0 nM LIN, 100.0 nM CHL, 100.0 nM MEPA, 100.0 nM MAL and 100.0 nM UA

electrochemical sensor has major advantages such as sensitivity with a limit of the detection value of 2.0×10^{-12} M, providing facile usage in food safety. Furthermore, in the presence of other interfering compounds, the suggested sensor demonstrated a considerable affinity for paraoxon. Thus, the proposed electrode based on MoS_2NPs@MWCNTs nanocomposite can be utilized to determine the environmental pollutants in practical applications. In addition, the produced nanocomposite results in better voltammetric improvement for the determination of complex samples. Finally, this study potentially opens the ground for the design and development of an exceedingly selective and sensitive electrochemical sensor for the detection of organophosphorus pesticides.

CRediT authorship contribution statement

Ömer Saltuk Bölükbaşı: Conceptualization, Methodology, Writing – review & editing. **Bahar Bankoğlu Yola:** Data curation, Visualization, Investigation. **Havva Boyacıoğlu:** Writing – original draft, Visualization, Investigation. **Mehmet Lütfi Yola:** Supervision, Conceptualization, Writing – review & editing.

Declaration of competing interest

The authors declare that they have no known competing financial interests or personal relationships that could have appeared to influence the work reported in this paper.

Appendix A. Supplementary data

Supplementary data to this article can be found online at https://doi.org/10.1016/j.fct.2022.112994.

References

Agui, L., Yanez-Sedeno, P., Pingarron, J.M., 2008. Role of carbon nanotubes in electroanalytical chemistry - a review. Anal. Chim. Acta 622, 11–47.
Arduini, F., Neagu, D., Scognamiglio, V., Patarino, S., Moscone, D., Palleschi, G., 2015. Automatable flow system for paraoxon detection with an embedded screen-printed electrode tailored with butyrylcholinesterase and prussian blue nanoparticles. Chemosensors 3, 129–145.
Bagheri, H., Afkhami, A., Khoshsafar, H., Hajian, A., Shahriyari, A., 2017. Protein capped Cu nanoclusters-SWCNT nanocomposite as a novel candidate of high performance platform for organophosphates enzymeless biosensor. Biosens. Bioelectron. 89, 829–836.
Beytur, M., Kardas, F., Akyildirim, O., Ozkan, A., Bankoglu, B., Yuksek, H., Yola, M.L., Atar, N., 2018. A highly selective and sensitive voltammetric sensor with molecularly imprinted polymer based silver@gold nanoparticles/ionic liquid modified glassy carbon electrode for determination of ceftizoxime. J. Mol. Liq. 251, 212–217.
Boke, C.P., Karaman, O., Medetalibeyoglu, H., Karaman, C., Atar, N., Yola, M.L., 2020. A new approach for electrochemical detection of organochlorine compound lindane: development of molecular imprinting polymer with polyoxometalate/carbon nitride nanotubes composite and validation. Microchem. J. 157, 105012.
Bravo, R., Driskell, W.J., Whitehead, R.D., Needham, L.L., Barr, D.B., 2002. Quantitation of dialkyl phosphate metabolites of organophosphate pesticides in human urine using GC-MS-MS with isotopic internal standards. J. Anal. Toxicol. 26, 245–252.
Costa, L.G., Giordano, G., Guizzetti, M., Vitalone, A., 2008. Neurotoxicity of pesticides: a brief review. Front Biosci-Landmrk 13, 1240–1249.
Dhull, V., 2020. A Nafion/AChE-cSWCNT/MWCNT/Au-based amperometric biosensor for the determination of organophosphorous compounds. Environ. Technol. 41, 566–576.
Gallardo, E., Barroso, M., Margalho, C., Cruz, A., Vieira, D.N., Lopez-Rivadulla, M., 2006. Determination of parathion in biological fluids by means of direct solid-phase microextraction. Anal. Bioanal. Chem. 386, 1717–1726.
Gopi, P.K., Ngo, D.B., Chen, S.M., Ravikumar, C.H., Surareungchai, W., 2022. High-performance electrochemical sensing of hazardous pesticide Paraoxon using BiVO4 nano dendrites equipped catalytic strips. Chemosphere 288, 132511.
Hryniewicz, B.M., Orth, E.S., Vidotti, M., 2018. Enzymeless PEDOT-based electrochemical sensor for the detection of nitrophenols and organophosphates. Sensor. Actuator. B Chem. 257, 570–578.
Hu, H.M., Huang, X.H., Deng, C.H., Chen, X.Y., Qian, Y.T., 2007. Hydrothermal synthesis of ZnO nanowires and nanobelts on a large scale. Mater. Chem. Phys. 106, 58–62.
Huang, K.J., Liu, Y.J., Wang, H.B., Wang, Y.Y., Liu, Y.M., 2014. Sub-femtomolar DNA detection based on layered molybdenum disulfide/multi-walled carbon nanotube composites, Au nanoparticle and enzyme multiple signal amplification. Biosens. Bioelectron. 55, 195–202.
Huang, K.J., Wang, L., Li, J., Liu, Y.M., 2013a. Electrochemical sensing based on layered MoS2-graphene composites. Sensor. Actuator. B Chem. 178, 671–677.
Huang, K.J., Wang, L., Liu, Y.J., Wang, H.B., Liu, Y.M., Wang, L.L., 2013b. Synthesis of polyaniline/2-dimensional graphene analog MoS2 composites for high-performance supercapacitor. Electrochim. Acta 109, 587–594.
Ioerger, B.P., Smith, J.S., 1993. Multiresidue method for the extraction and detection of organophosphate pesticides and their primary and secondary metabolites from beef tissue using hplc. J. Agric. Food Chem. 41, 303–307.
Karaman, C., Karaman, O., Atar, N., Yola, M.L., 2022a. A molecularly imprinted electrochemical biosensor based on hierarchical Ti2Nb10O29 (TNO) for glucose detection. Microchim. Acta 189, 1–11.
Karaman, O., Ozcan, N., Karaman, C., Yola, B.B., Atar, N., Yola, M.L., 2022b. Electrochemical cardiac troponin I immunosensor based on nitrogen and boron-doped graphene quantum dots electrode platform and Ce-doped SnO2/SnS2 signal amplification. Mater. Today Chem. 23, 100666.
Karimi-Maleh, H., Karimi, F., Fu, L., Sanati, A.L., Alizadeh, M., Karaman, C., Orooji, Y., 2022a. Cyanazine herbicide monitoring as a hazardous substance by a DNA nanostructure biosensor. J. Hazard Mater. 423, 127058.
Karimi-Maleh, H., Karimi, F., Fu, L., Sanati, A.L., Alizadeh, M., Karaman, C., Orooji, Y., 2022b. Cyanazine herbicide monitoring as a hazardous substance by a DNA nanostructure biosensor. J. Hazard Mater. 423.
Karimi-Maleh, H., Orooji, Y., Karimi, F., Alizadeh, M., Baghayeri, M., Rouhi, J., Tajik, S., Beitollahi, H.D., Agarwal, S., Gupta, V.K., Rajendran, S., Ayati, A., Fu, L., Sanati, A. L., Tanhaei, B., Sen, F., Shabani-nooshabadi, M., Asrami, P.N., Al-Othman, A., 2021a. A critical review on the use of potentiometric based biosensors for biomarkers detection. Biosens. Bioelectron. 184, 113252.
Karimi-Maleh, H., Yola, M.L., Atar, N., Orooji, Y., Karimi, F., Kumar, P.S., Rouhi, J., Baghayeri, M., 2021b. A novel detection method for organophosphorus insecticide

fenamiphos: molecularly imprinted electrochemical sensor based on core-shell Co3O4@MOF-74 nanocomposite. J. Colloid Interface Sci. 592, 174–185.
Khoshsafar, H., Karimian, N., Nguyen, T.A., Fakhri, H., Khanmohammadi, A., Hajian, A., Bagheri, H., 2022. Enzymeless voltammetric sensor for simultaneous determination of parathion and paraoxon based on Nd-based metal-organic framework. Chemosphere 292, 133440.
Kumaravel, A., Murugananthan, M., Mangalam, R., Jayakumar, S., 2020. A novel, biocompatible and electrocatalytic stearic acid/nanosilver modified glassy carbon electrode for the sensing of paraoxon pesticide in food samples and commercial formulations. Food Chem. 323, 126814.
Lahiff, E., Lynam, C., Gilmartin, N., O'Kennedy, R., Diamond, D., 2010. The increasing importance of carbon nanotubes and nanostructured conducting polymers in biosensors. Anal. Bioanal. Chem. 398, 1575–1589.
Lee, C., Yan, H., Brus, L.E., Heinz, T.F., Hone, J., Ryu, S., 2010. Anomalous lattice vibrations of single- and few-layer MoS2. ACS Nano 4, 2695–2700.
Li, J., Yang, Z.J., Tang, Y., Zhang, Y.C., Hu, X.Y., 2013a. Carbon nanotubes-nanoflake-like SnS2 nanocomposite for direct electrochemistry of glucose oxidase and glucose sensing. Biosens. Bioelectron. 41, 698–703.
Li, Y., Xu, C.Y., Hu, P.A., Zhen, L., 2013b. Carrier control of MoS2 nanoflakes by functional self-assembled monolayers. ACS Nano 7, 7795–7804.
Liu, Y.R., Hu, W.H., Li, X., Dong, B., Shang, X., Han, G.Q., Chai, Y.M., Liu, Y.Q., Liu, C.G., 2016. One-pot synthesis of hierarchical Ni2P/MoS2 hybrid electrocatalysts with enhanced activity for hydrogen evolution reaction. Appl. Surf. Sci. 383, 276–282.
Ma, G.F., Peng, H., Mu, J.J., Huang, H.H., Zhou, X.Z., Lei, Z.Q., 2013. In situ intercalative polymerization of pyrrole in graphene analogue of MoS2 as advanced electrode material in supercapacitor. J. Power Sources 229, 72–78.
Medetalibeyoglu, H., Beytur, M., Manap, S., Karaman, C., Kardas, F., Akyildirim, O., Kotan, G., Yuksek, H., Atar, N., Yola, M.L., 2020. Molecular imprinted sensor including Au nanoparticles/polyoxometalate/two-dimensional hexagonal boron nitride nanocomposite for diazinon recognition. Ecs J Solid State Sc 9, 101006.
Mohanraj, J., Durgalakshmi, D., Rakkesh, R.A., Balakumar, S., Rajendran, S., Karimi-Maleh, H., 2020. Facile synthesis of paper based graphene electrodes for point of care devices: a double stranded DNA (dsDNA) biosensor. J. Colloid Interface Sci. 566, 463–472.
Mulchandani, A., Chen, W., Mulchandani, P., Wang, J., Rogers, K.R., 2001. Biosensors for direct determination of organophosphate pesticides. Biosens. Bioelectron. 16, 225–230.
Ozkan, A., Atar, N., Yola, M.L., 2019. Enhanced surface plasmon resonance (SPR) signals based on immobilization of core-shell nanoparticles incorporated boron nitride nanosheets: development of molecularly imprinted SPR nanosensor for anticancer drug, etoposide. Biosens. Bioelectron. 130, 293–298.
Palleschi, G., Bernabei, M., Cremisini, C., Mascini, M., 1992. Determination of organophosphorus insecticides with a choline electrochemical biosensor. Sensor. Actuator. B Chem. 7, 513–517.
Paschoalin, R.T., Gomes, N.O., Almeida, G.F., Bilatto, S., Farinas, C.S., Machado, S.A., Mattoso, L.H., Oliveira Jr., O.N., Raymundo-Pereira, P.A., 2022. Wearable sensors made with solution-blow spinning poly (lactic acid) for non-enzymatic pesticide detection in agriculture and food safety. Biosens. Bioelectron. 199, 113875.
Pourabbas, B., Jamshidi, B., 2008. Preparation of MoS2 nanoparticles by a modified hydrothermal method and the photo-catalytic activity of MoS2/TiO2 hybrids in photo-oxidation of phenol. Chem. Eng. J. 138, 55–62.
Rajaji, U., Murugan, K., Chen, S.M., Govindasamy, M., Chen, T.W., Lin, P.H., Prabha, P. L., 2019. Graphene oxide encapsulated 3D porous chalcopyrite (CuFeS2) nanocomposite as an emerging electrocatalyst for agro-hazardous (methyl paraoxon) detection in vegetables. Compos. B Eng. 160, 268–276.
Raymundo-Pereira, P.A., Gomes, N.O., Shimizu, F.M., Machado, S.A.S., Oliveira, O.N., 2021. Selective and sensitive multiplexed detection of pesticides in food samples using wearable, flexible glove-embedded non-enzymatic sensors. Chem. Eng. J. 408, 127279.
Rezaei, H., Ardakani, S.J., Smith, K.J., 2012. Comparison of MoS2 catalysts prepared from Mo-micelle and Mo-octoate precursors for hydroconversion of cold lake vacuum residue: catalyst activity, coke properties and catalyst recycle. Energy Fuel. 26, 2768–2778.
Stoytcheva, M., Zlatev, R., Montero, G., Velkova, Z., Gochev, V., 2017. Nanostructured platform for the sensitive determination of paraoxon by using an electrode modified with a film of graphite-immobilized bismuth. Microchim. Acta 184, 2707–2714.
Verma, D., Chauhan, D., Das Mukherjee, M., Ranjan, K.R., Yadav, A.K., Solanki, P.R., 2021. Development of MWCNT decorated with green synthesized AgNps-based electrochemical sensor for highly sensitive detection of BPA. J. Appl. Electrochem. 51, 447–462.
Wang, G., Wang, Z.D., Zhang, Y.X., Fei, G.T., Zhang, L.D., 2004. Controlled synthesis and characterization of large-scale, uniform Dy(OH)(3) and DY2O3 single-crystal nanorods by a hydrothermal method. Nanotechnology 15, 1307–1311.
Xu, Q., Wang, S.F., 2005. Electrocatalytic oxidation and direct determination of L-tyrosine by square wave voltammetry at multi-wall carbon nanotubes modified glassy carbon electrodes. Microchim. Acta 151, 47–52.
Yadav, A.K., Verma, D., Solanki, P.R., 2021. Electrophoretically deposited L-cysteine functionalized MoS2@MWCNT nanocomposite platform: a smart approach toward highly sensitive and label-free detection of gentamicin. Mater. Today Chem. 22, 100567.
Yin, Z.Y., Li, H., Li, H., Jiang, L., Shi, Y.M., Sun, Y.H., Lu, G., Zhang, Q., Chen, X.D., Zhang, H., 2012. Single-layer MoS2 phototransistors. ACS Nano 6, 74–80.
Yola, M.L., Atar, N., Qureshi, M.S., Ustundag, Z., Solak, A.O., 2012. Electrochemically grafted etodolac film on glassy carbon for Pb(II) determination. Sensor. Actuator. B Chem. 171, 1207–1215.
Zhang, T.T., Zeng, L.X., Han, L., Li, T., Zheng, C., Wei, M.D., Liu, A.H., 2014. Ultrasensitive electrochemical sensor for p-nitrophenyl organophosphates based on ordered mesoporous carbons at low potential without deoxygenization. Anal. Chim. Acta 822, 23–29.